

Bayesian constraints on quark and neutron stars from multi-messenger observations

Wen-Jie Xie^{1,2,3,*} and Cheng-Jun Xia^{4,†}

¹*Department of Physics, Yuncheng University, Yuncheng 044000, China*

²*Shanxi Province Intelligent Optoelectronic Sensing Application Technology Innovation Center, Yuncheng University, Yuncheng 044000, China*

³*Guangxi Key Laboratory of Nuclear Physics and Nuclear Technology, Guangxi Normal University, Guilin 541004, China*

⁴*Center for Gravitation and Cosmology, College of Physical Science and Technology, Yangzhou University, Yangzhou 225009, China*

(Dated: July 1, 2025)

We constrain the quark matter equation of state (EOS) with color superconductivity (2SC, 2SC+s, CFL phases) and QCD corrections using Bayesian inference informed by multi-messenger observations from the NICER pulsars, HESS J1731-347 and GW170817. Our results reveal that the bag constant $B = 47\text{--}55 \text{ MeV/fm}^3$ are tightly constrained, the QCD correction strength a_4 is phase-dependent ($a_4 \approx 0.9$ for 2SC, ~ 0.6 for 2SC+s). A large surface tension is required for 2SC phase ($\sigma \gtrsim 95 \text{ MeV/fm}^2$) according to the stability constraints of ^{266}Hs . The mass-radius relations support quark stars as explanations for HESS J1731-347. The squared speed of sound converges to $c^2/3$, ruling out extreme stiffening. The inferred maximum quark star mass $M_{\text{max}} < 2.28 M_{\odot}$ (90% confidence level) rules out the secondary component of GW190814 ($2.59 \pm 0.08 M_{\odot}$) as a quark star. In particular, the quark stars (2SC phase) is strongly favored when including HESS J1731-347 data with the bayes factor $B_{2\text{SC}, \text{NS}} = 10.6$, but neutron stars are moderately preferred with $B_{\text{NS}, 2\text{SC}} = 3.22$ if HESS J1731-347 data is excluded. This demonstrates low-mass compact objects critically discriminate between quark matter phases and between quark and neutron-star models.

I. INTRODUCTION

Being one of the most dense objects in Universe, pulsar-like compact stars weigh $1\text{--}2 M_{\odot}$ but with radii being around 10 km, the average density of those objects thus easily surpass the nuclear saturation density $n_0 \approx 0.16 \text{ fm}^{-3}$. Traditionally, pulsar-like compact stars are thought to be made of $npe\mu$ matter fulfilling both charge neutrality and β -stability conditions, which is formed via core collapse supernovae. Due to the presence of strong gravitational field, the density at the center of compact stars may even exceeds $7\text{--}8n_0$, where a deconfinement phase transition is likely to take place and form quark matter (QM) in the core, i.e., hybrid stars. Nevertheless, consider the strangeness degree of freedom, the energy density of quark matter is reduced by converting u and d quarks into s quarks, which forms strange quark matter (SQM). It was found that SQM is more stable than nuclear matter in a large model space, i.e., the true QCD ground state [1–3]. In such cases, compact stars may in fact be strange quark stars comprised entirely of SQM [4–6]. In chiral models, nevertheless, SQM may be unstable due to a too large s quark mass [7, 8], while nonstrange quark matter ($ud\text{QM}$) could be more stable instead [9]. In such cases, compact stars could also be $ud\text{QM}$ stars [10–15]. Due to the attractive interaction among quarks, they are expected to pair and form various color superconducting phases in SQM and $ud\text{QM}$ [16], e.g., the two color-superconducting (2SC)

and color-flavor locked (CFL) phases. Beside forming pairs in momentum space, due to the strong interaction among quarks, they may even aggregate into quark clusters (strangeons) [17], where strangeon matter could be the true QCD ground state and compact stars may in fact be strangeon stars [18–20].

The most eminent differences between neutron stars (traditional neutron stars, hybrid stars, etc.) and strange stars (strange quark stars, $ud\text{QM}$ stars, strangeon stars, etc.) are their surface structures [21]. For example, neutron stars are gravity-bound with the density approaching to zero at their surfaces, beneath which are crusts made of crystalline structures. Consequently, there exist a minimum mass $M_{\text{min}} \approx 0.09 M_{\odot}$ for neutron stars with radius $R \approx 200\text{--}300 \text{ km}$ [22]. For strange stars, they are self-bound by the strong interaction among quarks or strangeons, where the density at the surface is typically few times the saturation density of nuclear matter and without a crust. In such cases, the mass and radius of a strange star can approach to zero as we decrease the central density. The mass-radius (M - R) relations for neutron stars and strange stars are thus distinctively different [23], which provide possibility to unveil the essence of pulsar-like compact stars according to recent astrophysical observations.

In particular, as we are in the multimessenger era, astrophysical constraints on pulsar-like compact stars have reached unprecedented accuracy. For example, by analyzing the arrival times of radio pulses from pulsars in a binary system, the masses of PSR J1614-2230 ($1.928 \pm 0.017 M_{\odot}$) [24, 25] and PSR J0348+0432 ($2.01 \pm 0.04 M_{\odot}$) have been measured [26]. The binary neutron star merger event GRB 170817A-GW170817-AT

* xiewenjie@ycu.edu.cn

† cjxia@yzu.edu.cn

2017gfo shows that the tidal deformability of $1.4M_\odot$ neutron star should lie within $70 \leq \Lambda_{1.4} \leq 580$ [27]. Employing pulse-profile modelings with the NICER and XMM-Newton data, the masses and radii of PSR J0030+0451, PSR J0740+6620, PSR J0437-4715, and PSR J1231-1411 have been measured [28–33]. Beside compact stars with $M > 1M_\odot$, there may exist compact objects with unusually small masses and radii, e.g., 4U 1746-37 [23] and the central compact object (CCO) within the supernova remnant HESS J1731-347 [34].

This work thus focuses on one of the most challenging puzzles in astrophysics: is the essence of pulsar-like compact objects a neutron star or a strange star? Based on the observational constraints of compact stars, we aim to constrain the EOSs of dense stellar matter and estimate the Bayesian evidences for neutron stars and strange stars in the framework of Bayesian inference approach. The paper is organized as follows. In Sec. II we present the theoretical framework for the EOS models of quark stars and neutron stars as well as the Bayesian inference approach. The obtained EOSs and structures of quark stars and neutron stars are presented in Sec. III, while the constraints and possible correlations among various parameters and quark matter properties are investigated. We draw our conclusion in Sec. IV

II. THEORETICAL FRAMEWORK

A. Quark star model

Since strange quark stars, $udQM$ stars, and strangeon stars share similar traits in their structures, as an example, in this work we consider quark stars with color superconductivity. Various theoretical models were proposed to describe the properties of quark matter in the literature, e.g., perturbation model [35–39], linear sigma model [9], MIT bag model [40, 41], Dyson-Schwinger equations [42, 43], equivparticle model [44, 45], quasiparticle model [46–48], and Nambu–Jona-Lasinio model [49]. Among these, the most widely used is the MIT bag model due to its simplicity and effectiveness in capturing certain essential features of QCD [40, 41]. In the present work, we use the approach presented in Refs. [14, 50]. The QM EOS can be expressed in terms of the pressure p and energy density ε as well as the four parameters B , Δ , m_s , and a_4 as

$$p = \frac{1}{3}(\varepsilon - 4B) + \frac{4\lambda^2}{9\pi^2} \left(-1 + (\lambda) \sqrt{1 + 3\pi^2 \frac{(\varepsilon - B)}{\lambda^2}} \right) \quad (1)$$

with

$$\lambda = \frac{c_1 \Delta^2 - c_2 m_s^2}{\sqrt{c_3 a_4}}, \quad (2)$$

where the parameter set (c_1, c_2, c_3) take the values (1.86, 1, 0) for the 2SC phase; (3, 1, 0.75) for the 2SC+s phase;

and (3, 3, 0.75) for the CFL phase, respectively [14]. The effective bag constant, B , which reflects the contributions of the QCD vacuum, is typically treated as a phenomenological parameter. Meanwhile, the parameter a_4 represents the QCD corrections arising from gluon-mediated interactions between quarks. It ranges from 0 to 1, where $a_4 = 1$ indicates the absence of QCD corrections, and $a_4 = 0$ signifies extremely strong QCD corrections [14, 41, 51–54]. The term involving the gap parameter Δ accounts for the effects of color superconductivity with Δ denoting the energy gap resulting from the quark pairing. m_s is the strange quark mass having a range of 90 to 100 MeV [55].

The above EOS expression (1) is derived from thermodynamic relations:

$$p = -\Omega, \quad n_q = -\frac{\partial \Omega}{\partial \mu}, \quad n_e = -\frac{\partial \Omega}{\partial \mu_e}, \quad \varepsilon = \Omega + n_q \mu + n_e \mu_e, \quad (3)$$

Here Ω denotes the free energy of the superconducting quark matter and can be written as [51, 52, 56]:

$$\Omega = -\frac{3a_4}{4\pi^2} \mu^4 - \frac{\mu_e^4}{12\pi^2} - \frac{12\Delta^2 - 3m_s^2}{4\pi^2} \mu^2 + B, \quad (4)$$

where μ_e is the electron chemical potential and $\mu = (\mu_u + \mu_d + \mu_s)/3$ the quark chemical potential with μ_u , μ_d and μ_s being the chemical potentials for u , d and s quark, respectively. The expressions (3) can be thus rewritten as:

$$n_q = \frac{3a_4}{\pi^2} \mu^3 + \frac{2\lambda\sqrt{3a_4}}{\pi^2} \mu, \quad n_e = \frac{\mu_e^3}{3\pi^2}, \quad (5)$$

$$\varepsilon = \frac{9a_4}{4\pi^2} \mu^4 + \frac{\mu_e^4}{4\pi^2} + B + \frac{\lambda\sqrt{3a_4}}{\pi^2} \mu^2. \quad (6)$$

The energy per baryon $\epsilon = 3\mu$ under the condition of $p = 0$ indicates the minimum energy per baryon [14], i.e.,

$$\epsilon = \frac{3\sqrt{2}\pi}{(c_1 a_4)^{1/4}} \frac{B^{1/4}}{\sqrt{\sqrt{4\bar{\lambda} + \pi^2} + 2\sqrt{\bar{\lambda}}}}, \quad (7)$$

with $\bar{\lambda} = \lambda^2/4B$. For quark stars to exist stably, the matter at their surfaces should be more stable than nuclear matter [1–3], i.e.,

$$\epsilon < \frac{M(^{56}\text{Fe})}{56}. \quad (8)$$

Meanwhile, since finite nuclei do not decay into $udQM$ nuggets, they should be unstable at $A \lesssim 300$ compared with that of finite nuclei. This condition provide additional constraints on $udQM$ and in particular the surface tension σ . If we demand the heaviest β -stable nucleus ^{266}Hs to be more stable than $udQM$ nuggets, the energy per baryon of $udQM$ in 2SC should fulfill the following stability constraint, i.e.,

$$\frac{M(^{266}\text{Hs})}{266} < \epsilon + \sigma \left(\frac{An_0^2}{36\pi} \right)^{-1/3}, \quad (9)$$

where the left hand side represents the energy per baryon for ^{266}Hs and on the right hand side a liquid-drop formula is employed with $A=266$ and $n_0 = n_q/3$ the saturation density of $ud\text{QM}$ at $\mu = \epsilon/3$ fixed by Eq. (7). This indicates a minimum value for σ at fixed bag model parameters B , Δ , and a_4 with $c_1 = 1.86$, $c_2 = 1$, and $c_3 = 0$ for the 2SC phase.

B. Neutron star model

In the framework of relativistic-mean-field (RMF) models, the Lagrangian density of density-dependent point-coupling model reads [57]

$$\mathcal{L} = \bar{\psi}(i\gamma^\mu\partial_\mu - M)\psi + \frac{1}{2}\alpha_S(\bar{\psi}\psi)^2 - \frac{1}{2}\alpha_V(\bar{\psi}\gamma^\mu\psi)^2 - \frac{1}{2}\alpha_{TV}(\bar{\psi}\gamma^\mu\tau_3\psi)^2. \quad (10)$$

where the four-fermion coupling constants α_S , α_V , and α_{TV} are density-dependent. The energy density of neutron star matter is then given by

$$\varepsilon = \varepsilon_k + \frac{1}{2}\alpha_S n_S^2 + \frac{1}{2}\alpha_V n_V^2 + \frac{1}{2}\alpha_{TV} n_{TV}^2, \quad (11)$$

where the kinetic energy density

$$\varepsilon_k = \sum_{i=p,n,e,\mu} \frac{m_i^{*4}}{8\pi^2} \left[x_i(2x_i^2 + 1)\sqrt{x_i^2 + 1} - \text{arcsinh}(x_i) \right]. \quad (12)$$

Here $x_i \equiv \nu_i/m_i^*$ with $m_{n,p}^* = m_{n,p} - \alpha_S n_S$ being the effective nucleon mass, $m_{e,\mu}^* = m_{e,\mu}$, and ν_i the Fermi momentum which determines the particle number density $n_i = \nu_i^3/3\pi^2$. The scalar and vector densities are fixed by

$$n_S = \sum_{i=n,p} \frac{m_i^{*3}}{2\pi^2} \left[x_i\sqrt{x_i^2 + 1} - \text{arcsinh}(x_i) \right], \quad (13)$$

$$n_V = n_n + n_p, \quad n_{TV} = n_n - n_p. \quad (14)$$

By fulfilling the charge neutrality and β -stability conditions at fixed density n_V , the number densities of protons, neutrons, electrons, and muons in neutron star matter can be fixed. The pressure is then obtained with

$$p = n_V \frac{d\varepsilon}{dn_V} - \varepsilon. \quad (15)$$

More details on the density-dependent formulae and derivations can be found in our previous publication [57].

C. Bayesian inference approach

The central concept of the Bayesian inference approach is the Bayes' theorem, which states:

$$P(\mathcal{M}|D) = \frac{P(D|\mathcal{M})P(\mathcal{M})}{\int P(D|\mathcal{M})P(\mathcal{M})d\mathcal{M}}. \quad (16)$$

In this context, $P(\mathcal{M}|D)$ denotes the posterior probability of the model \mathcal{M} given the dataset D , which is the central focus of our analysis. The term $P(D|\mathcal{M})$ refers to the likelihood function, representing the conditional probability that the model \mathcal{M} predicts the data D correctly. $P(\mathcal{M})$ is the prior probability of the model \mathcal{M} before considering the data. The denominator in Eq. (16), $\int P(D|\mathcal{M})P(\mathcal{M})d\mathcal{M}$, serves as a normalization constant, also known as the Bayesian evidence or marginal likelihood. This quantity enables the comparison of multiple models to determine which provides the best explanation for the experimental data, i.e., for the two models M_1 and M_2 , one can use the Bayes factor $B_{1,2}$ [58]

$$B_{1,2} = \frac{\int_{M_1} P(D|\mathcal{M}_1)P(\mathcal{M}_1)d\mathcal{M}_1}{\int_{M_2} P(D|\mathcal{M}_2)P(\mathcal{M}_2)d\mathcal{M}_2}. \quad (17)$$

A Bayes factor $B_{1,2} > 1$ indicates preference for M_1 , while $B_{1,2} < 1$ favors M_2 . Conventionally, $B_{1,2} > 3$ provides substantial evidence for M_1 ; $B_{1,2} > 10$ suggests strong evidence; $B_{1,2} > 30$ indicates very strong evidence; and $B_{1,2} > 100$ constitutes decisive evidence [58].

The model parameters and EOSs of neutron star matter were constrained in our previous publication [57], which will be not elaborated here. To investigate the EOS of quark matter and constrain the surface tension, we begin by randomly sampling four bag model parameters: B , Δ , m_s , and a_4 , while the surface tension σ is constrained according to Eq. (9) for 2SC phase. They are selected uniformly within the prior ranges provided in Table I. Once the parameters are chosen, we substitute them into the equations (2) and (3) to construct the EOS for quark matter. Following this, we proceed to determine the quark star (QS) mass-radius sequences by solving the Tolman-Oppenheimer-Volkoff (TOV) equations [59, 60], i.e.,

$$\frac{dp}{dr} = -\frac{GM\varepsilon}{r^2} \frac{(1+p/\varepsilon)(1+4\pi r^3 p/M)}{1-2GM/r}, \quad (18)$$

$$\frac{dM}{dr} = 4\pi r^2 \rho. \quad (19)$$

The gravitational constant is given by $G = 6.707 \times 10^{-45} \text{ MeV}^{-2}$. The dimensionless tidal deformability, Λ , is calculated using the following expression [61–64]:

$$\Lambda = \frac{2}{3}k_2 \left(\frac{R}{M} \right)^5, \quad (20)$$

where R and M are the radius and mass of the quark star, respectively. The second Love number, k_2 , is determined by the equation of state (EOS) and is governed by a set of coupled equations, specifically Eqs. (3)-(6) in Ref. [62], which are solved alongside the TOV equations with appropriate boundary conditions. The theoretical radius, $R_{\text{th},j}$, and tidal deformability, Λ_{th} , are then computed and used to assess the likelihood that the selected QS EOS can reproduce the observed values, $R_{\text{obs},j}$ and Λ_{obs} . Here, j represents the index of the data points,

as presented in Table II. The likelihood functions for the radius and tidal deformability are given by:

$$P_R[D(R_{1,2,\dots,n})|\mathcal{M}(p_{1,2,\dots,4})] = \prod_{j=1}^n \frac{\exp\left[-\frac{(R_{\text{th},j}-R_{\text{obs},j})^2}{2\sigma_{\text{obs},j}^2}\right]}{\sqrt{2\pi}\sigma_{\text{obs},j}}, \quad (21)$$

and

$$P_\Lambda[D(\Lambda)|\mathcal{M}(p_{1,2,\dots,4})] = \frac{1}{\sqrt{2\pi}\sigma_{\text{obs}}} \exp\left[-\frac{(\Lambda_{\text{th}}-\Lambda_{\text{obs}})^2}{2\sigma_{\text{obs}}^2}\right], \quad (22)$$

where $\sigma_{\text{obs},j}$ and σ_{obs} represent the 1σ error bars associated with the radius observation j and the tidal deformability, respectively. For data with different upper and lower 68% confidence boundaries (σ_{obs}), we treat them separately based on whether the observed radius R_{obs} is smaller or larger than the theoretical value. This allows us to approximate an asymmetric (non-Gaussian) distribution. Furthermore, when multiple results from different analyses of the same source (e.g., GW170817 or PSR J0030+0451) are available, we treat them as equally probable. In such cases, we compute their statistical average by randomly selecting one result with equal weight to calculate the likelihood function.

The total likelihood function is constructed by multiplying the individual likelihood components. In this work, we adopt the following expression for the total likelihood:

$$P[D|\mathcal{M}(p_{1,2,\dots,4})] = P_{\text{filter}} \times P_{\text{mass,max}} \times P_R \times P_\Lambda. \quad (23)$$

The component P_{filter} acts as a filter to select EOS parameter sets that satisfy the thermodynamic stability condition, i.e., $dP/dE \geq 0$; the causality condition, ensuring that the speed of sound is always less than the speed of light at all densities; the energy per baryon for quark matter is not greater than the one for the most stable nucleus ^{56}Fe , i.e., $\epsilon \leq 930$ MeV; The binding energy per baryon of ud QM nuggets must exceed 931.742 MeV at $A = 266$, i.e., fulfilling Eq. (9). The term $P_{\text{mass,max}}$ ensures that the EOS is sufficiently stiff to support the observational maximum mass of neutron stars, M_{max} . In this analysis, we adopt a value of $M_{\text{max}} = 1.97M_\odot$. To simulate the posterior probability density function (PDF) of the model parameters, we employ a Markov-Chain Monte Carlo (MCMC) method using the Metropolis-Hastings algorithm. This method allows us to sample the parameter space and derive the PDFs for individual parameters and their pairwise correlations by integrating over the other parameters. For instance, the PDF for the i th parameter, p_i , is defined as:

$$P(p_i|D) = \frac{\int P(D|\mathcal{M})dp_1dp_2\cdots dp_{i-1}dp_{i+1}\cdots dp_6}{\int P(D|\mathcal{M})P(\mathcal{M})dp_1dp_2\cdots dp_6}. \quad (24)$$

During the MCMC sampling, it is essential to discard the initial samples from the burn-in period, as the algorithm does not yet sample from the equilibrium distribution at the start. Based on our previous work, we find

that 40,000 burn-in steps are sufficient to reach equilibrium when the model contains six parameters [65–67]. Given that the current analysis involves only four parameters, this burn-in step count is more than adequate. Therefore, we discard the first 40,000 steps and utilize the remaining one million steps to compute the posterior PDFs of the four parameters in this analysis.

TABLE I. Prior ranges of the parameters used in this work.

Parameters	Lower limit	Upper limit
$B(\text{MeV}/\text{fm}^3)$	1	100
$\Delta(\text{MeV})$	0	100
a_4	0.1	1
$m_s(\text{MeV})$	90	100
$\sigma(\text{MeV}/\text{fm}^2)$	0	300

TABLE II. Data for a compact star's radius, mass and tidal deformability used in the present work.

Mass(M_\odot)	Radius R (km)	Source and Reference
$1.34^{+0.15}_{-0.16}$	$12.71^{+1.14}_{-1.19}$ (68% CI)	PSR J0030+0451 [28]
$1.44^{+0.15}_{-0.14}$	$13.0^{+1.2}_{-1.0}$ (68% CI)	PSR J0030+0451 [68]
$1.48^{+0.037}_{-0.037}$	$11.36^{+0.95}_{-0.63}$ (68% CI)	PSR J0437-4715 [32]
$2.08^{+0.07}_{-0.07}$	$13.7^{+2.6}_{-1.5}$ (68% CI)	PSR J0740+6620 [31]
$0.77^{+0.20}_{-0.17}$	$10.4^{+0.86}_{-0.78}$ (68% CI)	HESS J1731-347 [34]
$1.04^{+0.05}_{-0.03}$	$13.5^{+0.3}_{-0.5}$ (68% CI)	PSR J1231-1411 [33]
Mass(M_\odot)	Tidal deformability Λ	Source and Reference
1.4	190^{+390}_{-120} (90% CI)	GW170817 [69]

III. RESULTS AND DISCUSSION

Figure 1 demonstrates the quark star mass-radius (M - R) relations for the 2SC, 2SC+s, and CFL phases derived from the data outlined in Table II in the framework of the Bayesian inference approach. The results from NICER observations of PSR J0030+0451 [28, 30] and PSR J0740+6620 [29, 31], along with the M - R measurements of the compact object HESS J1731-347 [34] are included. It is found that the obtained M - R relations for quark stars agree with the observational constraints from PSR J0030+0451 and PSR J0740+6620. Notably, they can also describe the lower-mass object HESS J1731-347 with a certain probability. In contrast, the compact star masses and radii derived within a theoretical framework combining the RMF model with a Bayesian inference approach based on the same observational data as in Ref. [57], do not support the smaller-mass source HESS J1731-347, but remain consistent with the observations of PSR J0030+0451 and PSR J0740+6620. Furthermore, the M - R curves derived for the three quark matter phases—namely, 2SC, 2SC+s, and CFL—show no significant differences. This indicates that the vari-

TABLE III. Summary of posterior estimates for the five parameters, along with derived quantities of quark stars (radius and tidal deformability for 1.4 and 2.0 solar mass stars, maximum mass and the corresponding radius), central squared speed of sound, central pressure and central energy density for the CFL, 2SC+s and 2SC phases. Values are inferred using the combined datasets listed in Table II, and reported as median estimates with 68% and 90% credible intervals. Their prior ranges are indicated in Table I.

Parameters	68%			90%		
	CFL, 2SC+s, 2SC			CFL, 2SC+s, 2SC		
B (MeV/fm ³)	52.0 ^{+3.0} _{-3.0}	51.0 ^{+2.0} _{-3.0}	50.0 ^{+3.0} _{-3.0}	52.0 ^{+7.0} _{-5.0}	51.0 ^{+4.0} _{-3.0}	50.0 ^{+6.0} _{-4.0}
a_4	0.9 ^{+0.0} _{-0.3}	0.6 ^{+0.2} _{-0.1}	0.9 ^{+0.0} _{-0.1}	0.9 ^{+0.0} _{-0.4}	0.6 ^{+0.3} _{-0.1}	0.9 ^{+0.1} _{-0.1}
Δ (MeV)	77.0 ^{+1.0} _{-62.0}	32.0 ^{+32.0} _{-31.0}	94.0 ^{+5.0} _{-54.0}	77.0 ^{+6.0} _{-76.0}	32.0 ^{+57.0} _{-32.0}	94.0 ^{+4.0} _{-83.0}
m_s (MeV)	98.0 ^{+0.0} _{-6.5}	99.5 ^{+0.0} _{-6.5}	91.0 ^{+6.0} _{-0.5}	98.0 ^{+1.5} _{-7.0}	99.5 ^{+0.0} _{-9.0}	91.0 ^{+8.0} _{-0.5}
σ (MeV/fm ²)	130.0 ^{+75.0} _{-125.0}	110.0 ^{+125.0} _{-75.0}	135.0 ^{+125.0} _{-40.0}	130.0 ^{+155.0} _{-110.0}	110.0 ^{+175.0} _{-90.0}	135.0 ^{+160.0} _{-65.0}
$R_{1.4}$ (km)	12.7 ^{+0.2} _{-0.2}	12.8 ^{+0.2} _{-0.2}	12.7 ^{+0.2} _{-0.2}	12.7 ^{+0.5} _{-0.3}	12.7 ^{+0.5} _{-0.3}	12.8 ^{+0.4} _{-0.3}
$R_{2.0}$ (km)	13.0 ^{+0.4} _{-0.1}	13.0 ^{+0.4} _{-0.1}	13.1 ^{+0.3} _{-0.2}	13.0 ^{+0.6} _{-0.3}	13.0 ^{+0.6} _{-0.3}	13.1 ^{+0.5} _{-0.4}
$\Lambda_{1.4}$	675.0 ^{+90.0} _{-45.0}	675.0 ^{+90.0} _{-45.0}	675.0 ^{+90.0} _{-45.0}	675.0 ^{+135.0} _{-135.0}	675.0 ^{+180.0} _{-45.0}	675.0 ^{+180.0} _{-45.0}
$\Lambda_{2.0}$	70.0 ^{+15.0} _{-10.0}	70.0 ^{+15.0} _{-5.0}	80.0 ^{+10.0} _{-15.0}	70.0 ^{+30.0} _{-10.0}	70.0 ^{+30.0} _{-10.0}	80.0 ^{+25.0} _{-15.0}
M_{\max} (M_{\odot})	2.185 ^{+0.04} _{-0.04}	2.165 ^{+0.055} _{-0.02}	2.2 ^{+0.025} _{-0.055}	2.185 ^{+0.085} _{-0.045}	2.165 ^{+0.1} _{-0.025}	2.2 ^{+0.075} _{-0.055}
R_{\max} (km)	12.3 ^{+0.3} _{-0.15}	12.25 ^{+0.3} _{-0.15}	12.3 ^{+0.3} _{-0.15}	12.3 ^{+0.5} _{-0.25}	12.25 ^{+0.55} _{-0.15}	12.3 ^{+0.5} _{-0.25}
v_s^2	0.336 ^{+0.001} _{-0.002}	0.336 ^{+0.001} _{-0.001}	0.334 ^{+0.003} _{-0.0}	0.336 ^{+0.004} _{-0.002}	0.336 ^{+0.001} _{-0.002}	0.334 ^{+0.004} _{-0.001}
p_c (MeV)	256.0 ^{+8.0} _{-8.0}	256.0 ^{+0.0} _{-16.0}	256.0 ^{+0.0} _{-16.0}	256.0 ^{+8.0} _{-24.0}	256.0 ^{+8.0} _{-16.0}	256.0 ^{+8.0} _{-24.0}
ε_c (MeV/fm ³)	968.0 ^{+8.0} _{-64.0}	960.0 ^{+16.0} _{-48.0}	960.0 ^{+8.0} _{-64.0}	968.0 ^{+24.0} _{-88.0}	960.0 ^{+24.0} _{-80.0}	960.0 ^{+24.0} _{-88.0}

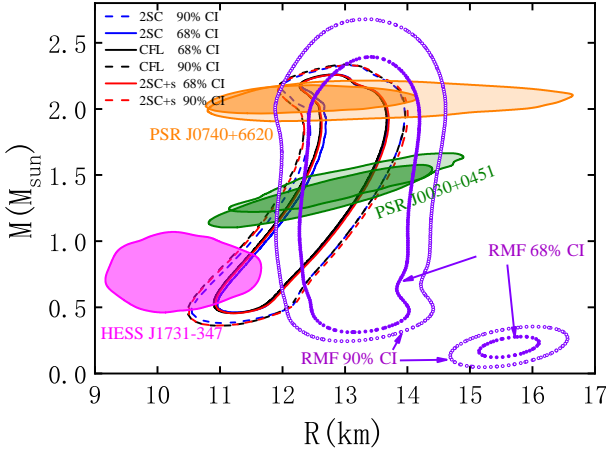


FIG. 1. (color online) Mass-radius posterior PDFs derived from the datasets in Table II at 68% (90%) confidence level shown by solid curves (dashed curves) for the CFL, 2SC+s, and 2SC phases, while these of neutron stars are indicated as well (RMF). For comparison, the results from the NICER observations of PSR J0030+0451 [28, 30] and PSR J0740+6620 [29, 31], as well as the HESS J1731-347 [34] are included.

ations in their internal equations of state have minimal impact on the macroscopic properties of quark stars.

Figure 2 presents the posterior distribution functions for five parameters involved in the QM EOS for the 2SC, 2SC+s, and CFL phases, and their correlations at 90% confidence level derived through a Bayesian statistical framework combining the MIT bag model with the ob-

servational data. These include radii, tidal deformabilities for 1.4 and 2.0 times the solar mass, maximum mass, and the corresponding radius. For comparison, the constraints on the parameters B , a_4 and Δ from Refs. [41] and [70] are also presented in the figure, demonstrating general agreement with our findings. Regarding the bag parameter B , the 68% credible intervals (CIs) for the three phases are $52.0^{+3.0}_{-3.0}$, $51.0^{+2.0}_{-3.0}$ and $50.0^{+3.0}_{-3.0}$ in units of MeV/fm³ as summarized in Table III, respectively, indicating minimal variation. In contrast, significant differences emerge for a_4 . For the 2SC phase (which does not incorporate strange quarks), with the additional stability constraint of ^{266}Hs in Eq. (9), current astrophysical observations provide tight constraints and yield $a_4 = 0.9^{+0.0}_{-0.1}$; these data favor larger a_4 values while showing minimal sensitivity to Δ and m_s . The surface tension σ is also constrained for the 2SC phase, where Eq. (9) indicates a lower limit for σ . Relative to its prior range of 0–300 MeV/fm² listed in Table I, the current data constrain σ weakly, yielding a 68% credible interval of $135.0^{+125.0}_{-40.0}$ MeV/fm², where the lower limit increases with a_4 . Note that the upper limit for σ is in fact unconstrained. Weak correlations exist among all parameters, except for a positive correlation emerging between the bag parameter B and the gap parameter Δ . However, this positive correlation becomes significantly weakened for the 2SC+s phase, which is consistent with the results in Ref. [70].

Figure 3 displays the posterior PDFs of macroscopic properties for quark stars, including the maximum mass and its radius, radii and tidal deformabilities of 1.4 M_{\odot} and 2.0 M_{\odot} stars, central energy density, central pressure, and central speed of sound. The results indicate

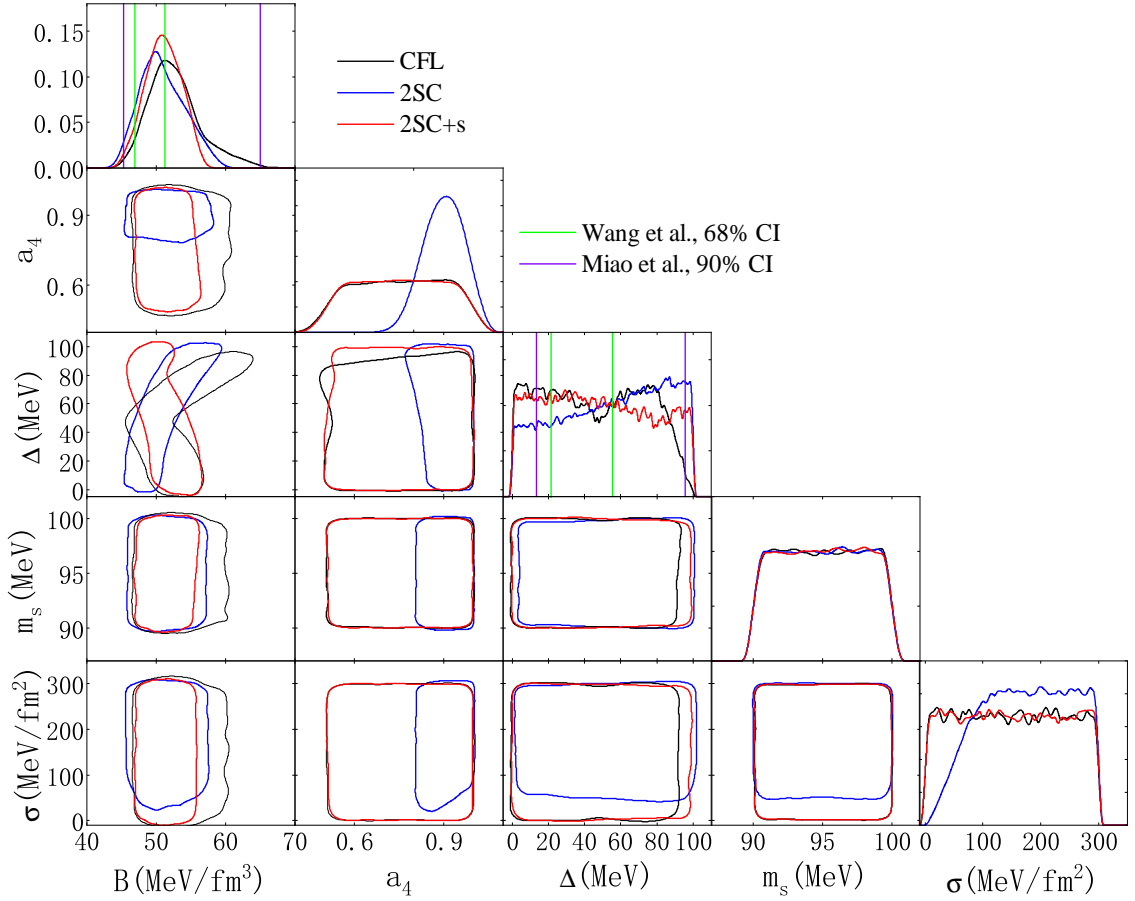


FIG. 2. (color online) Posterior probability distribution functions of the five parameters for the QM EOS and their correlations inferred from the Bayesian analysis of the data listed in Table II. For comparison, these by Miao et al. in Ref. [41] and by Wang et al. in Ref. [70] are included.

minimal differences among the three quark matter phases (2SC, 2SC+s, CFL) for these observables. The derived maximum stellar mass is less than approximately $2.35 M_{\odot}$, which excludes the possibility that the secondary component of the gravitational-wave event GW190814 is a quark star in the MIT bag model.

The extreme EOS in the cores of compact stars, representing the densest matter environments in the Universe, plays a pivotal role in understanding strong interaction physics and general relativistic effects. There have been numerous prior discussions suggesting that, in order to satisfy the lower-mass limit of two solar masses for compact stars, the value of v_s in compact-star matter should significantly surpass the conformal limit of $c/\sqrt{3}$ [36, 71–73]. In some studies, i.e., see [74], it has even been observed to be close to $0.9c$ around $5n_0$ with $n_0 \approx 0.16 \text{ fm}^{-3}$ being the saturation density. These results align with theoretical predictions from perturbative QCD [75] and Bayesian analyses incorporating multi-messenger data [76, 77]. Our analysis demonstrates v_s^2 values clustered near $1/3$, with $0.336^{+0.001}_{-0.002}$, $0.336^{+0.001}_{-0.001}$, $0.334^{+0.003}_{-0.0}$ (68% CI) for CFL,

2SC+s, and 2SC phases, respectively, consistent with the constraints from Ref. [41]. Notably, the results by considering strange quarks, i.e., CFL and 2SC+s phases, show higher probability densities for $v_s^2 > 1/3$.

Central EOS parameters, the core pressure (p_c) and energy density (ε_c), also exhibit same PDFs for the three phases. The bimodal ε_c distributions suggest significant influence from low-mass star observations of HESS J1731-347 [34]. At 68% confidence level, for CFL phase for example, $p_c = 256.0^{+8.0}_{-8.0} \text{ MeV}$ and $\varepsilon_c = 968.0^{+8.0}_{-64.0} \text{ MeV/fm}^3$. These results agree with perturbative TOV equation analyses [78], which reports $\varepsilon_c = 901^{+214}_{-287} \text{ MeV/fm}^3$, $p_c = 218^{+93}_{-125} \text{ MeV}$, though our constraints are markedly narrower.

Figures 4 and 5 respectively illustrate the equations of state (relationship between pressure and energy density) for three quark phases, and the variation of squared speed of sound with energy density. From Fig. 4, it can be observed that the EOS for quark matter composed of these three quark phases are nearly identical, and an outcome consistent with theoretical expectations, as also evidenced in the preceding three figures. Moreover, cur-

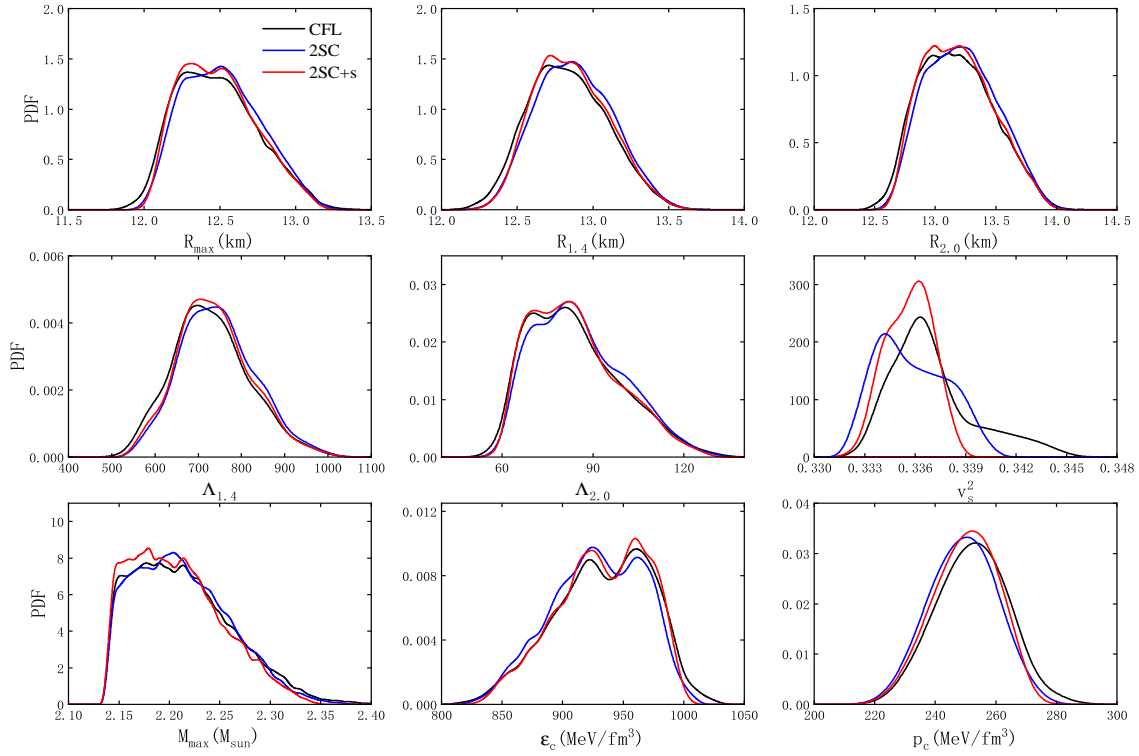


FIG. 3. (color online) Posterior probability distribution functions of the radius, tidal deformability corresponding to the quark stars with 1.4 and 2.0 solar masses, maximum mass and the corresponding radius, central squared speed of sound, central energy density and central pressure inferred from the Bayesian analysis of the data listed in Table II for the CFL, 2SC and 2SC+s phases.

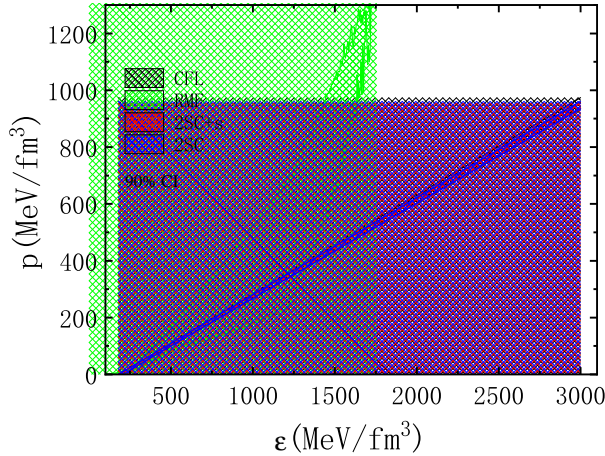


FIG. 4. (color online) Posterior probability distribution functions of the QM EOS (90% confidence level) for the CFL, 2SC and 2SC+s phases inferred from the Bayesian analysis of the dataset listed in Table II.

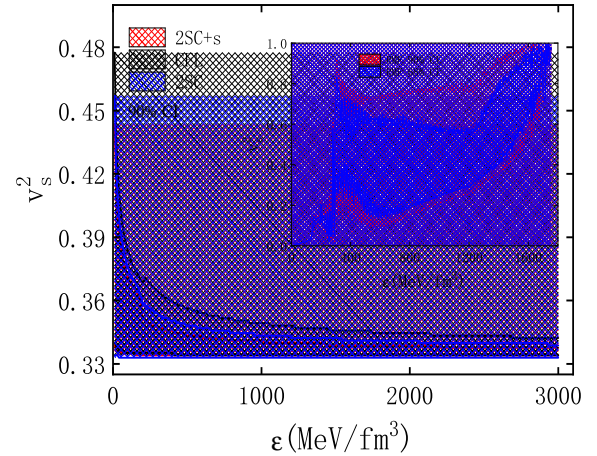


FIG. 5. (color online) As with Fig. 1, but showing the posterior probability distribution functions of the squared speed of sound v_s^2 vs. energy density ϵ relation.

rent observational data effectively constrain the EOSs for quark star matter. In Fig. 5, the squared speed of sound slightly decreases with increasing energy density, approaching the conformal limit of $1/3$. Among the three

quark phases, the CFL phase exhibits the largest variation range in squared sound speed, followed by the 2SC phase, while the 2SC+s phase shows the smallest variation. For comparison, the results of neutron star matter

from RMF models are also incorporated in the figures, where speed of sound is much larger than the conformal limit.

TABLE IV. The Bayesian evidence for the QM EOSs of 2SC, 2SC+s and CFL phases as well as the neutron-star (NS) EOS using the relativistic mean-field model in Ref. [57].

	w/ HESS J1731-347	w/o HESS J1731-347
2SC	14.14	101.2
2SC+s	5.88	40.15
CFL	6.43	42.22
NS	1.33	325.9

In Table IV, we presents the Bayesian evidence for the EOSs derived from three quark phases (calculated via the MIT bag model used in the present work) and the neutron star EOSs (calculated by the relativistic mean-field model used in Ref. [57]), under two observational constraints: with and without the HESS J1731-347 source. We can have the following important observations:

1. Quark stars: For both data scenarios, the 2SC phase exhibits significantly higher Bayesian evidence than the other quark phases.
 - With HESS J1731-347: The Bayes factors $B_{2SC,2SC+s} = 2.4$ and $B_{2SC,CFL} = 2.2$.
 - Without HESS J1731-347: $B_{2SC,2SC+s} = 2.5$ and $B_{2SC,CFL} = 2.4$. The Bayesian evidence for the 2SC+s and CFL phases is comparable.
2. Quark stars vs. neutron stars:
 - With HESS: Quark stars (2SC phase) are strongly favored over neutron stars, with $B_{2SC,NS} = 10.6$.
 - Without HESS: Neutron stars are moderately favored over the quark stars (2SC phase), with $B_{NS,2SC} = 3.22$.

IV. CONCLUSION

In this study, we established robust constraints on the QM EOS incorporating color superconductivity and QCD corrections, utilizing a Bayesian framework informed by multi-messenger observations of compact stars. Our analysis employs the MIT bag model extended to include color-superconducting phases (2SC, 2SC+s, CFL), with parameters sampled over physically motivated priors. By synthesizing data from NICER (PSR J0030+0451, PSR J0740+6620), HESS J1731-347, and gravitational-wave event GW170817, we derived posterior distributions for the EOS parameters and key macroscopic properties of quark stars. Key findings are summarized as follows:

1. Parameter constraints:

(i) The bag constant B is tightly constrained to 47–55 MeV/fm³ (68% CI) across all phases, consistent with perturbative QCD expectations.

(ii) The QCD correction strength a_4 exhibits phase dependence: $a_4 \approx 0.9$ for 2SC (favoring weak corrections and large surface tensions with $\sigma \gtrsim 95$ MeV/fm²), while lower values ($a_4 \approx 0.6$) are permitted in 2SC+s.

(iii) The strange quark mass m_s ($m_s \sim 90$ –100 MeV) and the superconducting gap Δ show broad posteriors ($\Delta \sim 0$ –100 MeV), indicating observational insensitivity.

2. Macroscopic star properties:

(i) The mass-radius relations are consistent with NICER and HESS J1731-347 data. Radii for $1.4M_\odot$ and $2.0M_\odot$ stars cluster at 12.7–13.1 km (68% CI), with tidal deformabilities $\Lambda_{1.4} \approx 675$ and $\Lambda_{2.0} \approx 70$ –80.

(ii) The maximum quark star masses are $M_{\max} \lesssim 2.28M_\odot$ (90% CI), excluding the $2.6M_\odot$ secondary component of GW190814 as a quark star.

(iii) The squared sound speed v_s^2 converges to 0.334–0.336 near the conformal limit 1/3, supporting asymptotic freedom in dense QCD matter.

3. Phase dependence and model selection:

(i) EOS and macroscopic properties show minimal variation among phases (CFL, 2SC+s, 2SC), implying limited sensitivity of current data to internal quark pairing structures.

(ii) The Bayesian evidence strongly favors quark stars (2SC phase) when including HESS J1731-347 data ($B_{2SC,NS} = 10.6$), but neutron stars become preferred if this low-mass source is excluded. This highlights the critical role of low-mass compact objects in distinguishing quark and neutron-star matter models.

ACKNOWLEDGMENTS

The authors would like to thank Dr. Chen Zhang and Prof. Renxin Xu for fruitful discussions. C.J.X. is supported by the National SKA Program of China (Grant No. 2020SKA0120300) and the National Natural Science Foundation of China (Grant No. 12275234). W.J.X. is supported by the Open Project of Guangxi Key Laboratory of Nuclear Physics and Nuclear Technology under Grant No. NLK2023-03, and the Central Government Guidance Funds for Local Scientific and Technological Development, China, under Grant No. Guike ZY22096024.

-
- [1] A. R. Bodmer, Collapsed nuclei, *Phys. Rev. D* **4**, 1601 (1971).
- [2] E. Witten, Cosmic separation of phases, *Phys. Rev. D* **30**, 272 (1984).
- [3] H. Terazawa, Super-hypernuclei in the quark-shell model, *J. Phys. Soc. Jpn.* **58**, 3555 (1989).
- [4] N. Itoh, Hydrostatic equilibrium of hypothetical quark stars, *Prog. Theor. Phys.* **44**, 291 (1970).
- [5] C. Alcock, E. Farhi, and A. Olinto, Strange stars, *Astrophys. J.* **310**, 261 (1986).
- [6] P. Haensel, J. L. Zdunik, and R. Schaeffer., Strange quark stars, *Astron. Astrophys.* **160**, 121 (1986).
- [7] M. Buballa and M. Oertel, Strange quark matter with dynamically generated quark masses, *Phys. Lett. B* **457**, 261 (1999).
- [8] T. Klähn and T. Fischer, Vector interaction enhanced bag model for astrophysical applications, *Astrophys. J.* **810**, 134 (2015).
- [9] B. Holdom, J. Ren, and C. Zhang, Quark matter may not be strange, *Phys. Rev. Lett.* **120**, 222001 (2018).
- [10] C.-J. Xia, S.-S. Xue, R.-X. Xu, and S.-G. Zhou, Super-critically charged objects and electron-positron pair creation, *Phys. Rev. D* **101**, 103031 (2020).
- [11] T. Zhao, W. Zheng, F. Wang, C.-M. Li, Y. Yan, Y.-F. Huang, and H.-S. Zong, Do current astronomical observations exclude the existence of nonstrange quark stars?, *Phys. Rev. D* **100**, 043018 (2019).
- [12] C. Zhang, Probing up-down quark matter via gravitational waves, *Phys. Rev. D* **101**, 043003 (2020).
- [13] Z. Cao, L.-W. Chen, P.-C. Chu, and Y. Zhou, Gw190814: Circumstantial evidence for up-down quark star, *Phys. Rev. D* **106**, 083007 (2022).
- [14] C. Zhang and R. B. Mann, Unified interacting quark matter and its astrophysical implications, *Phys. Rev. D* **103**, 063018 (2021).
- [15] W.-L. Yuan, A. Li, Z. Miao, B. Zuo, and Z. Bai, Interacting ud and uds quark matter at finite densities and quark stars, *Phys. Rev. D* **105**, 123004 (2022).
- [16] M. G. Alford, A. Schmitt, K. Rajagopal, and T. Schäfer, Color superconductivity in dense quark matter, *Rev. Mod. Phys.* **80**, 1455 (2008).
- [17] R.-X. Xu, Solid quark stars?, *Astrophys. J.* **596**, L59 (2003).
- [18] X. Y. Lai and R. X. Xu, Lennard-Jones quark matter and massive quark stars, *Mon. Not. Roy. Astron. Soc.* **398**, L31 (2009).
- [19] X. Y. Lai, C. Y. Gao, and R. X. Xu, H-cluster stars, *Mon. Not. R. Astron. Soc.* **431**, 3282 (2013).
- [20] Z.-Q. Miao, C.-J. Xia, X.-Y. Lai, T. Maruyama, R.-X. Xu, and E.-P. Zhou, A bag model of matter condensed by the strong interaction, *Int. J. Mod. Phys. E* **31**, 2250037 (2022).
- [21] X. Lai and R. Xu, Strangeon and strangeon star, *J. Phys: Conf. Ser.* **861**, 012027 (2017).
- [22] P. Haensel, J. L. Zdunik, and F. Douchin, Equation of state of dense matter and the minimum mass of cold neutron stars, *A&A* **385**, 301 (2002).
- [23] Z.-S. Li, Z.-J. Qu, L. Chen, Y.-J. Guo, J.-L. Qu, and R.-X. Xu, An ultra-low-mass and small-radius compact object in 4u 1746-37?, *Astrophys. J.* **798**, 56 (2015).
- [24] P. B. Demorest, T. Pennucci, S. M. Ransom, M. S. E. Roberts, and J. W. T. Hessels, A two-solar-mass neutron star measured using Shapiro delay, *Nature* **467**, 1081 (2010).
- [25] E. Fonseca, T. T. Pennucci, J. A. Ellis, I. H. Stairs, D. J. Nice, S. M. Ransom, P. B. Demorest, Z. Arzoumanian, K. Crowter, T. Dolch, R. D. Ferdman, M. E. Gonzalez, G. Jones, M. L. Jones, M. T. Lam, L. Levin, M. A. McLaughlin, K. Stovall, J. K. Swiggum, and W. Zhu, The nanograv nine-year data set: Mass and geometric measurements of binary millisecond pulsars, *Astrophys. J.* **832**, 167 (2016).
- [26] J. Antoniadis, P. C. C. Freire, N. Wex, T. M. Tauris, R. S. Lynch, M. H. van Kerkwijk, M. Kramer, C. Bassa, V. S. Dhillon, T. Driebe, J. W. T. Hessels, V. M. Kaspi, V. I. Kondratiev, N. Langer, T. R. Marsh, M. A. McLaughlin, T. T. Pennucci, S. M. Ransom, I. H. Stairs, J. van Leeuwen, J. P. W. Verbiest, and D. G. Whelan, A massive pulsar in a compact relativistic binary, *Science* **340**, 1233232 (2013).
- [27] LIGO Scientific and Virgo Collaborations, Gw170817: Measurements of neutron star radii and equation of state, *Phys. Rev. Lett.* **121**, 161101 (2018).
- [28] T. E. Riley, A. L. Watts, S. Bogdanov, P. S. Ray, R. M. Ludlam, S. Guillot, Z. Arzoumanian, C. L. Baker, A. V. Bilous, D. Chakrabarty, K. C. Gendreau, A. K. Harding, W. C. G. Ho, J. M. Lattimer, S. M. Morsink, and T. E. Strohmayer, A nicer view of psr j0030+0451: Millisecond pulsar parameter estimation, *Astrophys. J.* **887**, L21 (2019).
- [29] T. E. Riley, A. L. Watts, P. S. Ray, S. Bogdanov, S. Guillot, S. M. Morsink, A. V. Bilous, Z. Arzoumanian, D. Choudhury, J. S. Deneva, K. C. Gendreau, A. K. Harding, W. C. G. Ho, J. M. Lattimer, M. Loewenstein, R. M. Ludlam, C. B. Markwardt, T. Okajima, C. Prescod-Weinstein, R. A. Remillard, M. T. Wolff, E. Fonseca, H. T. Cromartie, M. Kerr, T. T. Pennucci, A. Parthasarathy, S. Ransom, I. Stairs, L. Guillemot, and I. Cognard, A NICER view of the massive pulsar PSR j0740+6620 informed by radio timing and XMM-newton spectroscopy, *Astrophys. J.* **918**, L27 (2021).
- [30] M. C. Miller, F. K. Lamb, A. J. Dittmann, S. Bogdanov, Z. Arzoumanian, K. C. Gendreau, S. Guillot, A. K. Harding, W. C. G. Ho, J. M. Lattimer, R. M. Ludlam, S. Mahmoodifar, S. M. Morsink, P. S. Ray, T. E. Strohmayer, K. S. Wood, T. Enoto, R. Foster, T. Okajima, G. Prigozhin, and Y. Soong, Psr j0030+0451 mass and radius from nicer data and implications for the properties of neutron star matter, *Astrophys. J.* **887**, L24 (2019).
- [31] M. C. Miller, F. K. Lamb, A. J. Dittmann, S. Bogdanov, Z. Arzoumanian, K. C. Gendreau, S. Guillot, W. C. G. Ho, J. M. Lattimer, M. Loewenstein, S. M. Morsink, P. S. Ray, M. T. Wolff, C. L. Baker, T. Cazeau, S. Manthripragada, C. B. Markwardt, T. Okajima, S. Pollard, I. Cognard, H. T. Cromartie, E. Fonseca, L. Guillemot, M. Kerr, A. Parthasarathy, T. T. Pennucci, S. Ransom, and I. Stairs, The radius of PSR j0740+6620 from NICER and XMM-newton data, *Astrophys. J.* **918**, L28 (2021).
- [32] D. Choudhury, T. Salmi, S. Vinciguerra, T. E. Riley, Y. Kini, A. L. Watts, B. Dorsman, S. Bogdanov, S. Guil-

- lot, P. S. Ray, D. J. Reardon, R. A. Remillard, A. V. Bilous, D. Huppenkothen, J. M. Lattimer, N. Rutherford, Z. Arzoumanian, K. C. Gendreau, S. M. Morsink, and W. C. G. Ho, A nicer view of the nearest and brightest millisecond pulsar: Psr j0437-4715, *Astrophys. J. Lett.* **971**, L20 (2024).
- [33] T. Salmi, J. S. Deneva, P. S. Ray, A. L. Watts, D. Choudhury, Y. Kini, S. Vinciguerra, H. T. Cromartie, M. T. Wolff, Z. Arzoumanian, S. Bogdanov, K. Gendreau, S. Guillot, W. C. G. Ho, S. M. Morsink, I. Cognard, L. Guillemot, G. Theureau, and M. Kerr, A nicer view of psr j1231-1411: A complex case, *Astrophys. J.* **976**, 58 (2024).
- [34] V. Doroshenko, V. Suleimanov, G. Pühlhofer, and A. Santangelo, A strangely light neutron star within a supernova remnant, *Nat. Astron.* **6**, 1444 (2022).
- [35] E. S. Fraga, A. Kurkela, and A. Vuorinen, Interacting quark matter equation of state for compact stars, *Astrophys. J.* **781**, L25 (2014).
- [36] A. Kurkela, E. S. Fraga, J. Schaffner-Bielich, and A. Vuorinen, Constraining neutron star matter with quantum chromodynamics, *Astrophys. J.* **789**, 127 (2014).
- [37] J. F. Xu, G. X. Peng, F. Liu, D.-F. Hou, and L.-W. Chen, Strange matter and strange stars in a thermodynamically self-consistent perturbation model with running coupling and running strange quark mass, *Phys. Rev. D* **92**, 025025 (2015).
- [38] C.-J. Xia and S.-G. Zhou, Stable strange quark matter objects with running masses and coupling constant, *Nucl. Phys. B* **916**, 669 (2017).
- [39] C.-J. Xia, T. Maruyama, N. Yasutake, and T. Tatsumi, Constraining quark-hadron interface tension in the multimessenger era, *Phys. Rev. D* **99**, 103017 (2019).
- [40] E.-P. Zhou, X. Zhou, and A. Li, Constraints on interquark interaction parameters with gw170817 in a binary strange star scenario, *Phys. Rev. D* **97**, 083015 (2018).
- [41] Z. Miao, J.-L. Jiang, A. Li, and L.-W. Chen, Bayesian inference of strange star equation of state using the GW170817 and GW190425 data, *Astrophys. J.* **917**, L22 (2021).
- [42] C. D. Roberts and A. G. Williams, Dyson-schwinger equations and their application to hadronic physics, *Prog. Part. Nucl. Phys.* **33**, 477 (1994).
- [43] R. Alkofer and L. von Smekal, The infrared behaviour of qcd green's functions: Confinement, dynamical symmetry breaking, and hadrons as relativistic bound states, *Phys. Rep.* **353**, 281 (2001).
- [44] G. X. Peng, A. Li, and U. Lombardo, Deconfinement phase transition in hybrid neutron stars from the brueckner theory with three-body forces and a quark model with chiral mass scaling, *Phys. Rev. C* **77**, 065807 (2008).
- [45] C. J. Xia, G. X. Peng, S. W. Chen, Z. Y. Lu, and J. F. Xu, Thermodynamic consistency, quark mass scaling, and properties of strange matter, *Phys. Rev. D* **89**, 105027 (2014).
- [46] R. D. Pisarski, Renormalized fermion propagator in hot gauge theories, *Nucl. Phys. A* **498**, 423 (1989).
- [47] K. Schertler, C. Greiner, and M. H. Thoma, Strange matter with effective quark masses, *J. Phys. G* **23**, 2051 (1997).
- [48] K. Schertler, C. Greiner, and M. Thoma, Medium effects in strange quark matter and strange stars, *Nucl. Phys. A* **616**, 659 (1997).
- [49] M. Buballa, Njl-model analysis of dense quark matter, *Phys. Rep.* **407**, 205 (2005).
- [50] J. P. Pereira, C. V. Flores, and G. Lugones, Phase transition effects on the dynamical stability of hybrid neutron stars, *Astrophys. J.* **860**, 12 (2018).
- [51] E. S. Fraga, R. D. Pisarski, and J. Schaffner-Bielich, Small, dense quark stars from perturbative qcd, *Phys. Rev. D* **63**, 121702 (2001).
- [52] M. Alford, M. Braby, M. Paris, and S. Reddy, Hybrid stars that masquerade as neutron stars, *Astrophys. J.* **629**, 969 (2005).
- [53] S. Bhattacharyya, I. Bombaci, D. Logoteta, and A. V. Thampan, Fast spinning strange stars: possible ways to constrain interacting quark matter parameters, *Mon. Not. R. Astron. Soc.* **457**, 3101 (2016).
- [54] A. Li, Z.-Y. Zhu, and X. Zhou, New equations of state for postmerger supramassive quark stars, *Astrophys. J.* **844**, 41 (2017).
- [55] Particle Data Group, Review of particle physics, *Chin. Phys. C* **38**, 090001 (2014).
- [56] S. Weissenborn, I. Sagert, G. Pagliara, M. Hempel, and J. Schaffner-Bielich, Quark matter in massive compact stars, *Astrophys. J.* **740**, L14 (2011).
- [57] C.-J. Xia, W.-J. Xie, and M. Bakhiet, Astrophysical constraints on nuclear eoss and coupling constants in relativistic-mean-field models, *Phys. Rev. D* **110**, 114009 (2024).
- [58] J. Lattimer and A. Steiner, Constraints on the symmetry energy using the mass-radius relation of neutron stars, *Eur. Phys. J. A* **50**, 40 (2014).
- [59] R. C. Tolman, Effect of inhomogeneity on cosmological models, *Proc. Nat. Acad. Sci.* **20**, 169 (1934).
- [60] J. R. Oppenheimer and G. M. Volkoff, On massive neutron cores, *Phys. Rev.* **55**, 374 (1939).
- [61] F. J. Fattoyev, J. Carvajal, W. G. Newton, and B.-A. Li, Constraining the high-density behavior of the nuclear symmetry energy with the tidal polarizability of neutron stars, *Phys. Rev. C* **87**, 015806 (2013).
- [62] T. Malik, N. Alam, M. Fortin, C. Providência, B. K. Agrawal, T. K. Jha, B. Kumar, and S. K. Patra, Gw170817: Constraining the nuclear matter equation of state from the neutron star tidal deformability, *Phys. Rev. C* **98**, 035804 (2018).
- [63] T. Hinderer, B. D. Lackey, R. N. Lang, and J. S. Read, Tidal deformability of neutron stars with realistic equations of state and their gravitational wave signatures in binary inspiral, *Phys. Rev. D* **81**, 123016 (2010).
- [64] T. Hinderer, Tidal love numbers of neutron stars, *Astrophys. J.* **677**, 1216 (2008).
- [65] W.-J. Xie and B.-A. Li, Bayesian inference of high-density nuclear symmetry energy from radii of canonical neutron stars, *Astrophys. J.* **883**, 174 (2019).
- [66] W.-J. Xie and B.-A. Li, Bayesian inference of the symmetry energy of superdense neutron-rich matter from future radius measurements of massive neutron stars, *Astrophys. J.* **899**, 4 (2020).
- [67] W.-J. Xie, Z.-W. Ma, and J.-H. Guo, Bayesian inference of the crust-core transition density via the neutron-star radius and neutron-skin thickness data, *Nucl. Sci. Tech.* **34**, 91 (2023).
- [68] E. Fonseca, H. T. Cromartie, T. T. Pennucci, P. S. Ray, A. Y. Kirichenko, S. M. Ransom, P. B. Demorest, I. H. Stairs, Z. Arzoumanian, L. Guillemot, A. Parthasarathy,

- M. Kerr, I. Cognard, P. T. Baker, H. Blumer, P. R. Brook, M. DeCesar, T. Dolch, F. A. Dong, E. C. Ferrara, W. Fiore, N. Garver-Daniels, D. C. Good, R. Jennings, M. L. Jones, V. M. Kaspi, M. T. Lam, D. R. Lorimer, J. Luo, A. McEwen, J. W. McKee, M. A. McLaughlin, N. McMann, B. W. Meyers, A. Naidu, C. Ng, D. J. Nice, N. Pol, H. A. Radovan, B. Shapiro-Albert, C. M. Tan, S. P. Tendulkar, J. K. Swiggum, H. M. Wahl, and W. W. Zhu, Refined mass and geometric measurements of the high-mass PSR j0740+6620, *Astrophys. J.* **915**, L12 (2021).
- [69] LIGO Scientific and Virgo Collaborations, Properties of the binary neutron star merger gw170817, *Phys. Rev. X* **9**, 011001 (2019).
- [70] Z. Wang, Y. Gao, D. Liang, J. Zhao, and L. Shao, Vetting quark-star models with gravitational waves in the hierarchical bayesian framework, *J. Cosmol. Astropart. P.* **2024**, 038 (2024).
- [71] P. Bedaque and A. W. Steiner, Sound velocity bound and neutron stars, *Phys. Rev. Lett.* **114**, 031103 (2015).
- [72] J. Alsing, H. O. Silva, and E. Berti, Evidence for a maximum mass cut-off in the neutron star mass distribution and constraints on the equation of state, *Mon. Not. Roy. Astron. Soc.* **478**, 1377 (2018).
- [73] B.-J. Cai, B.-A. Li, and Z. Zhang, Central speed of sound, the trace anomaly, and observables of neutron stars from a perturbative analysis of scaled tolmán-oppenheimer-volkoff equations, *Phys. Rev. D* **108**, 103041 (2023).
- [74] I. Tews, J. Margueron, and S. Reddy, Critical examination of constraints on the equation of state of dense matter obtained from gw170817, *Phys. Rev. C* **98**, 045804 (2018).
- [75] C.-J. Xia, Z. Zhu, X. zhou, and A. Li, Sound velocity in dense stellar matter with strangeness and compact stars, *Chin. Phys. C* **45**, 055104 (2021).
- [76] A. Li, Z. Miao, S. Han, and B. Zhang, Constraints on the maximum mass of neutron stars with a quark core from gw170817 and nicer psr j0030+0451 data, *Astrophys. J.* **913**, 27 (2021).
- [77] P. Landry, R. Essick, and K. Chatzioannou, Nonparametric constraints on neutron star matter with existing and upcoming gravitational wave and pulsar observations, *Phys. Rev. D* **101**, 123007 (2020).
- [78] B.-J. Cai, B.-A. Li, and Z. Zhang, Core states of neutron stars from anatomizing their scaled structure equations, *Astrophys. J.* **952**, 147 (2023).